



ARTICLE

Green Synthesis of Silver Nanoparticles Using *Plectranthus Amboinicus* Leaf Extract for Preparation of CMC/PVA Nanocomposite Film

Nguyen Thi Thanh Thuy^{1,*}, Le Hoang Huy¹, Truong Thuy Vy¹, Nguyen Thi Thanh Tam², Bien Thi Lan Thanh¹ and Nguyen Thi My Lan³

¹Nong Lam University Ho Chi Minh City, Ho Chi Minh City, 700000, Vietnam

²Industrial University of Ho Chi Minh City, Ho Chi Minh City, 700000, Vietnam

³University of Science, Viet Nam National University Ho Chi Minh City, Ho Chi Minh City, 700000, Vietnam

*Corresponding Author: Nguyen Thi Thanh Thuy. Email: nguyenthanhthuy@hcmuaf.edu.vn

Received: 12 January 2021 Accepted: 13 February 2021

ABSTRACT

In the present study, the biogenic silver nanoparticles have been synthesized using aqueous leaf extract of *Plectranthus amboinicus* (PA), which acted as both reducing and stabilizing agents. The PA synthesized silver nanoparticles were blended with carboxymethyl cellulose/polyvinyl alcohol (CMC/PVA) biocomposite. The prepared AgNPs as well as the biogenic AgNPs incorporated CMC/PVA films were investigated using UV-visible spectrophotometry, Fourier-transform infrared spectroscopy (FT-IR), dynamic light scattering (DLS), scanning electron microscope (SEM), and X-ray diffraction (XRD). The DLS results showed that biogenic AgNPs had the average particle size of 65.70 nm with polydispersity index of 0.44. The surface plasmon resonance of AgNPs, which was determined by UV-vis spectrophotometry, showed the value of 410.00 nm. These results therefore confirmed the reduction Ag^+ into Ag^0 and the formation of AgNPs in the medium. The SEM imaging showed that AgNPs was quasi-spherical and monodisperse. The XRD peaks at 33.07°, 44.19°, 64.58° and 77.47° confirmed the crystalline nature and presence of AgNPs. The CMC/PVA films that incorporated with AgNPs displayed best mechanical strength and morphological properties than the pure CMC/PVA film. The film of CMC/PVA-AgNPs exhibited significant antibacterial activities against *Bacillus spizizenii*, *Staphylococcus aureus*, *Salmonella typhi* and *Escherichia Coli*.

KEYWORDS

Carboxymethyl cellulose; antibacterial; green synthesis; silver nanoparticles; *plectranthus amboinicus*; polyvinyl alcohol

1 Introduction

In recent years, biosynthesis of nanocomposites films has attracted tremendous interest because of its biocompatibility, biodegradability, antimicrobial, and physical properties [1]. In nanocomposites films, the biopolymer has been combined with inorganic fillers that have one dimension in nanometer scale, such as metals and metal oxides, which act not only as an active ingredient but also as the reinforcing function [2–4]. The properties of nanocomposites depend on the type of fillers nanoparticles because of their shape and size, their concentration, and their interactions with the biopolymer matrix. Therefore, these nanocomposites might have advantages of both the properties of biopolymer and inorganic materials,



which are viable alternatives to traditional materials for numerous applications. Among the many inorganic materials, silver nanoparticles are one of the most important types of nanoparticles that are used in improving the polymer composites properties due to their unique physicochemical properties [5]. Silver nanoparticles are usually synthesized using chemical reduction [6], electrochemical method [7] or thermal decomposition [8]. However, these methods require hazardous and carcinogenic chemicals, such as sodium citrate, hydrazine, potassium bitartrate and some toxic solvents, such as sodium dodecyl, benzyl sulphate, and poly (vinyl pyrrolidone). Recently, considerable efforts have been made to use alternative chemicals that are less toxic and more environmentally friendly for the synthesis of AgNPs. Among them, plant-based chemicals show to be the promising resources that could be used in the synthesis method. Until now, a variety of plant extracts has been studied such as *Maclura pomifera* [9], *Givotia moluccana* [10], *Thymus kotschyanus* [11], *Mulberry* [12], green tea [13], *Crocus haussknechtii bois* [14], *Senna siamea* [15], and *Fritillaria* [16]. Silver nanoparticles are extensively used for a wide range of applications, such as antibacterial agents [17,18], sensors [19], surface enhanced Raman scattering (SERS) [20], and catalysts [21]. Furthermore, antibacterial activities are one of the most promising applications of AgNPs due to their broad-spectrum effect against both Gram negative and Gram positive bacteria. In particular, AgNPs display effective activities against resistance bacteria [22]. Many studies have showed that the silver ions (Ag^+) released from AgNPs can attach to the cell wall of bacteria, cause cell destruction and ultimately lead to cell death [23,24]. In addition, AgNPs can modify the three-dimensional structure of proteins by forming chemical bonds between Ag^+ and thiol (-SH) groups in protein molecules. The malformed proteins may have adverse effects on protein synthesis, DNA replication and disruption of cellular function [25]. Moreover, the advantage of AgNPs is that they can be easily incorporated to several polymers such as polyethylene glycol, polyvinylchloride, polyvinyl alcohol, cellulose, starch, and chitosan for many applications in food packaging, clothing industry, biomedicine, and production of biomaterials [26,27].

Carboxymethyl cellulose (CMC) is a biodegradable and biocompatible anionic polymer that can be employed for biotechnological and pharmaceutical applications. On the other hand, CMC is a biopolymer that retains various desirable characteristics, such as non-toxic, water-soluble, low-cost, emulsification, gelation, and excellent film forming [28]. Additionally, CMC is used as a suspending, thickening agent and a binder in the food and the pharmaceutical industry owing to its high water absorbing capacity. Different from carboxymethyl cellulose, polyvinyl alcohol (PVA) is a semi-crystalline plastic, biocompatible, hydroxyl rich, non-toxic and hydrophilic polymer. PVA is a synthetic polymer that is water-soluble and has excellent film forming properties. Due to its excellent properties, PVA is extensively used not only in food packaging, but also in many applications, such as paper coating, construction sectors, textile sizing [29]. Even though PVA is widely used in the development of food packaging film, it has poor stability, swelling in water and lack of antimicrobial properties. To overcome this crisis, PVA is blended with other polymer like CMC, chitosan, cellulose, etc. For example, it can be modified by CMC due to the hydrogen bonding between the OH groups in PVA and the carboxymethyl groups in CMC [30]. Hydrogen bonding interactions provide well dispersion of nanofillers in the polymer matrix, which is a crucial factor determining the polymer nanocomposites properties [31]. Inorganic nanoparticles reinforced polymer composites is an effective method to enhance the properties of the polymer matrix. The mixture of AgNPs as nanofillers for polymer blend to prepare the nanocomposites might improve not only the prepared polymer nanocomposites properties like thermal, mechanical and optical properties but also produce extra functions and various applications in the pharmaceutical and food industries. In recent years, the polymer composites compounding with metallic nanofillers have been used as ideal polymeric packaging films for the food product and polymeric wound dressing membranes for the treatment of skin wounds [32,33]. For instance, Rolim et al. [34] used poly(vinyl alcohol) and poly(ethylene glycol) to synthesize PVA/PEG films containing AgNPs and GSNO (the NO donor S-nitroglutathione) that exhibited potential antimicrobial and antitumorigenic activity. In another study,

Batool et al. [35] used a casting method to synthesize nanocomposites films consisting of PVA, starch and AgNPs. The results showed that the synthesized PVA/Starch-AgNPs exhibited good antibacterial activity against *E.coli* with potential application as the wound dressing membranes. Augustine et al. [36] indicated that PVA/bAg membranes containing about 0.25% to 1% bAg nanoparticles can be used for the development of antibacterial wound dressings. Ghaffari-Moghaddam et al. [37] fabricated nanocomposites based on polyaniline/polyvinyl alcohol/Ag (PANI/PVA/Ag). The results indicated that PANI/PVA/Ag membranes displayed effective antibacterial activity against Gram-positive bacteria *Staphylococcus aureus* and Gram-negative *Escherichia coli*. Zulkifli et al. [38] used the electrospinning method to synthesize the CMC/PVA/AgNPs fibers based on different concentration of AgNO₃ (0.6%–2.0%). The authors concluded that the CMC/PVA/AgNPs scaffold films were potential for wound healing and tissue engineering application.

The objective of this research was to synthesize a biodegradable carboxymethyl cellulose/polyvinyl alcohol-biogenic silver nanocomposite film for food packaging applications. The silver nanoparticles were synthesized using the extract of *Plectranthus amboinicus* as reducing and stabilizing agents. The antibacterial activity of nanocomposite film was studied against *Bacillus spizizenii*, *Staphylococcus aureus*, *Salmonella typhi* and *Escherichia Coli* by the disk diffusion method.

2 Materials and Methods

2.1 Materials

Silver nitrate used in this work was purchased from Merck, Germany. Poly(vinyl alcohol) (Mn 20,000–30,000 k by GPC) was purchased from Acros, Belgium. All chemicals used for the experiment were purchased from Acors. *Plectranthus amboinicus* (PA) leaves were collected from local market in Ho Chi Minh City, Vietnam. Deionized water was used in all the experiments.

2.2 Microorganisms

The antibacterial activity of prepared nanocomposites was determined using four different bacterial strains including Gram-positive (*Bacillus spizizenii* and *Staphylococcus aureus*), and Gram-negative (*Salmonella typhi* and *Escherichia Coli*). All the bacterial strains were obtained from Department of Biotechnology, Nong Lam University Ho Chi Minh City, Vietnam.

2.3 Preparation of *Plectranthus Amboinicus* Leaf Extract (PA)

PA leaves were rinsed three times with deionized water and then air-dried at room temperature. 25 g of leaves were then grinded in 100 mL of deionized water, followed by incubation at 60°C and gentle agitation for 1 h. The mixture was subsequently filtered through a Whatman No. 1 filter paper and then centrifuged at 10,000 rpm for 10 min. The aqueous extract was collected and stored at 4°C until it was used as a reducing and stabilizing agent in the following experiments.

2.4 Synthesis of Biogenic Silver Nanoparticles (AgNPs) from PA Leaf Extract

Synthesis of AgNPs was carried out following the method described by Mankad et al. [39] with some modifications. Firstly, 2 mL of the leaf extract of PA were mixed with 20 mL of a AgNO₃ aqueous solution in a 250 mL round-bottom flask. The round-bottom flask was covered with an aluminum foil and then stirred with a magnetic bar at room temperature until the colour changes from colorless to dark brown, indicating the formation of AgNPs. To study the optimization of biogenic silver nanoparticles synthesis, four parameters were carried out like the volume of PA leaf extract, silver nitrate (AgNO₃) concentration, stirring speed and time of reaction. The resulting AgNPs were collected by centrifugation at 10,000 rpm and washed several times with deionized water and then with ethanol to obtain pure AgNPs. The harvested pellet was dried in a hot air oven for 50°C for 24 h.

2.5 Characterization of AgNPs

The biosynthesized silver nanoparticles were characterized using a Visible Spectrophotometer (Genesys 20, Thermo Scientific Genesys, USA). The surface plasmon resonance (SPR) was analyzed by scanning the sample at the wavelength of 200 nm–800 nm. The FTIR spectra were carried out on a FTIR spectrophotometer (Nicolet, Impact 410, Madison, WI, USA), using KBr pellets. The spectra were measured between 400 and 4000 cm^{-1} . Scanning electron microscopy (SEM) (SU 8010, Hitachi, Japan) was used to analyze the morphology of the synthesized AgNPs. The elemental composition of AgNPs-PA was obtained by EDS analysis. The crystallite phase of AgNPs was identified by recording X-ray diffraction patterns (XRD) using a X-ray diffractometer with Cu- α radiation source (Shimadzu XRD-6000, Japan). The hydrodynamic diameter of PA synthesized AgNPs was determined using a dynamic light scattering (DLS) (Zetasizer Nano, Malvern, UK) at a fixed scattering angle of 90°C at 25°C.

2.6 Preparation of CMC/PVA-AgNPs Films

Synthesis of CMC/PVA-AgNPs films were carried out by a solvent casting method, as shown in Fig. 1. Initially, PVA solution was prepared by taking 2.5 g of poly(vinyl alcohol) (PVA) in a 100 mL beaker with 50 mL of distilled water and heated at 80°C under stirring by a magnetic stirrer for 60 min. The PVA solution was then cooled down to the room temperature. At the same time, carboxymethyl cellulose (CMC) was added in a beaker containing 50 mL of distilled water under constant stirring for 60 min and to this solution, the newly biosynthesized AgNPs and PVA solution were added and the crosslinking agent (0.3 g of acid citric) with the plasticizer (0.2 g of glycerol) was added to PVA/CMC-AgNPs mixture. After that, the solution mixture was heated at 60°C for 5 h under constant stirring. The whole mixture was sonicated for 20 min to remove air bubbles and the resulting produce was casted into glass Petri dishes and dried in oven at 50°C for 24 h. As a control, CMC/PVA film without silver nanoparticles was also prepared in a similar procedure as CMC/PVA-AgNPs film.

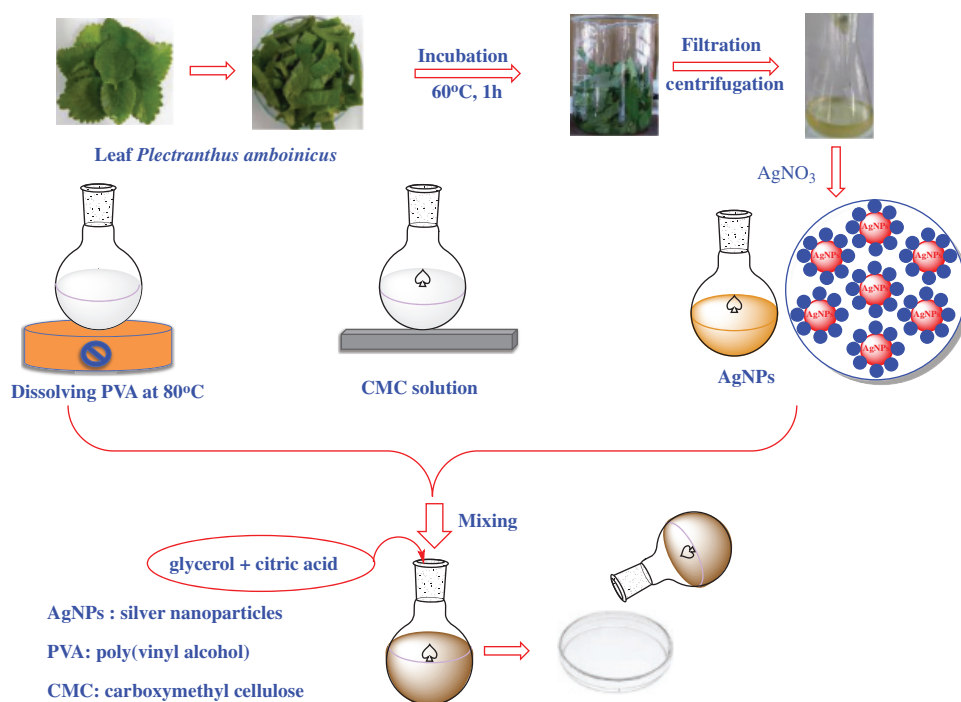


Figure 1: A preparation process of CMC/PVA and CMC/PVA-AgNPs films

2.7 Characterization of CMC/PVA-AgNPs Films

2.7.1 Thickness

The film thickness was measured at room temperature with a hand-held micrometer. Thickness was measured at five random positions and average film thickness was calculated.

2.7.2 Mechanical Properties

Tensile strength of the films was determined using Texture Analyzer TA-HD plus according to standard ASTM D882. The film samples were cut into 6 cm × 1 cm and fixed between grips of the instrument, stretched at a rate of 20 mm/min until breaking. Tensile strength and break elongation were expressed in MPa and percentage (%), respectively. All the measurements were done at least five replicates.

2.7.3 Antibacterial Activity Test

The antibacterial activities of CMC/PVA with and without AgNPs were tested against Gram-positive bacteria (*Bacillus spizizenii* and *Staphylococcus aureus*), and Gram-negative bacteria (*Salmonella typhi* and *Escherichia Coli*) using an agar well diffusion assay [40]. All the bacteria tested were grown overnight in 5 mL of lysogeny broth (LB) medium, with the exception of *Staphylococcus aureus*, which was grown in brain-heart medium. The assays were conducted using 100 µL of the overnight bacterial cultures (10^6 – 10^7 CFU mL⁻¹). Bacteria were spread to Petri plates containing brain-heart agar medium (for *S. aureus*) or LB medium (for other bacteria). Then, the agar medium was punctured to form 3 wells (8 mm in diameter) and the films were cut into slices and then added into each well. Three replicates were used for CMC/PVA-AgNPs films. Antibacterial activity was measured by observing the size of the inhibition zone formed around the well after incubation at 37°C for 24 h.

3 Results and Discussion

Initially, the colors of CMC/PVA films showed transparent, then its colors turned to yellowish after containing biosynthesized silver nanoparticles. Films formed from CMC/PVA and CMC/PVA-AgNPs are represented in Fig. 2.

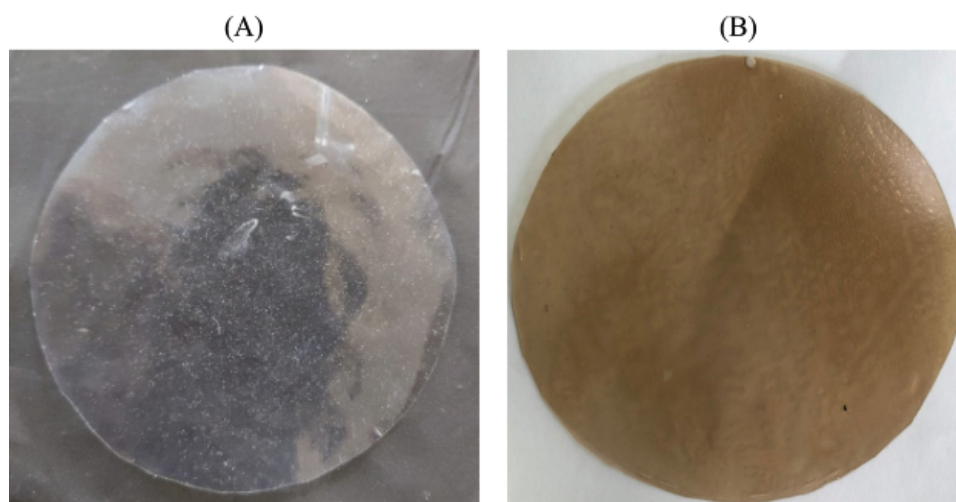


Figure 2: CMC/PVA (A) and CMC/PVA-AgNPs (B) films

The biosynthesized AgNPs as well as the fabricated nanocomposite films were fully characterized using UV-vis, FT-IR, DLS, SEM-EDX techniques.

3.1 Biogenic Silver Nanoparticles Synthesis Optimization

The formation of silver nanoparticles (AgNPs) was evidenced by a color change in the reaction mixture and confirmed by UV-vis Spectrophotometry at the wavelength of 200 nm–800 nm. After adding the *Plectranthus amboinicus* (PA) leaf extract into silver nitrate (AgNO_3), the solution color turned from transparent to dark brown (Fig. 3A). The color changes of AgNO_3 solution might result from the presence of the other chemical compounds in the plant extract such as carvacrol, alkaloids, thymol, and phenoplasts [41]. These compounds also played a significant role as stabilizing agents to stabilize the formed AgNPs. The UV-vis spectrum of PA leaf extract did not show a peak whereas that of *Plectranthus amboinicus* AgNPs (AgNPs-PA) showed a single surface Plasmon's resonance (SPR) band with a maximum wavelength (λ_{max}) at 400 nm–450 nm (Fig. 3B), which indicated the formation of AgNPs-PA [42]. The UV-vis results were consistent with previous studies on the biosynthesis of AgNPs [43,44]. The effects of extract volume of PA, silver nitrate concentration, the stirring rate, and the stirring time on the AgNPs formation are shown in Fig. 4. An increase of the intensity of SPR absorption bands with an increasing extract volume from 0.5 mL to 1.5 mL was observed (Fig. 4A). However, higher volume of aqueous extract led to a decrease of the SPR absorption due to the colloid dilution. Accordingly, the volume of 1.5 mL PA extract was chosen as the optimum extract volume for the AgNPs formation process. Fig. 4B also shows the effects of the time contact to synthesized AgNPs. The intensity of absorption band increased with the increasing of the time stirring up to 45 min, and had no significant difference between 60 min and 75 min, confirmed that the time reaction was completed at 60 min. The UV-vis spectrum of biogenic silver nanoparticles in different stirring rate showed that the SPR intensity peak was rising with the increase in the stirring rate up to 750 rpm (Fig. 4C). It was clearly indicated that the stirring rate could accelerate the rate of reaction. However, higher stirring rate led to a decrease in the SPR absorption and attributed to some aggregations of formed biogenic AgNPs. This may be explained due to the vigorous stirring leading to the damage active site of biomolecules in the aqueous extract of PA, breaking the AgNPs structure and reducing the efficiency of the synthesis process. Thus, the stirring rate of 750 rpm was considered as the optimum for the biosynthesis of AgNPs. The AgNO_3 concentration also played an important role in the synthesized AgNPs process because it affected the formation of AgNPs (Fig. 4D). The intensity of the SPR absorption was risen by the increase in the concentration of AgNO_3 from 0.5 mM to 2.0 mM, and hence started to reduce from 2.5 mM due to the insufficient amount of PA extract needed to reduce silver ions (Ag^+) to a silver atom (Ag^0). From the UV-vis study the 2.0 mM of AgNO_3 concentration showed the maximum peak among the all concentration of AgNO_3 and chosen for the future work. In general, the optimum conditions for these biogenic AgNPs were 1.5 mL of PA extract, 60 min of the stirring time, 750 rpm of the stirring rate, and 2.0 mM of AgNO_3 concentration.

3.2 Characteristics of the Synthesized AgNPs-PA

3.2.1 FT-IR Spectroscopy

The FT-IR spectra of AgNPs-PA showed the characteristic bands of PA leaf extract. As observed on Fig. 5, the FT-IR spectra of PA showed the same prominent peaks at 3448 cm^{-1} (-NH stretching of secondary amide or O-H stretching of alcohol or phenol groups), 2093 cm^{-1} (O-H stretching of carboxylic groups, H-bonded), 1638 cm^{-1} (C=O stretching vibration of aromatic ketones or carboxyl groups), and 1080 cm^{-1} (C-OH stretching of secondary alcohols or primary aliphatic amines) [45]. However, the FT-IR spectra of biogenic AgNPs-AP indicated weak signals, demonstrated that the components of PA extract had reacted to form AgNPs. These results revealed that the plant extract contain several functional groups such as -OH, -CHO, C=O, NH_2 and C=N, which are important for the reduction and stabilization of the biosynthesized AgNPs.

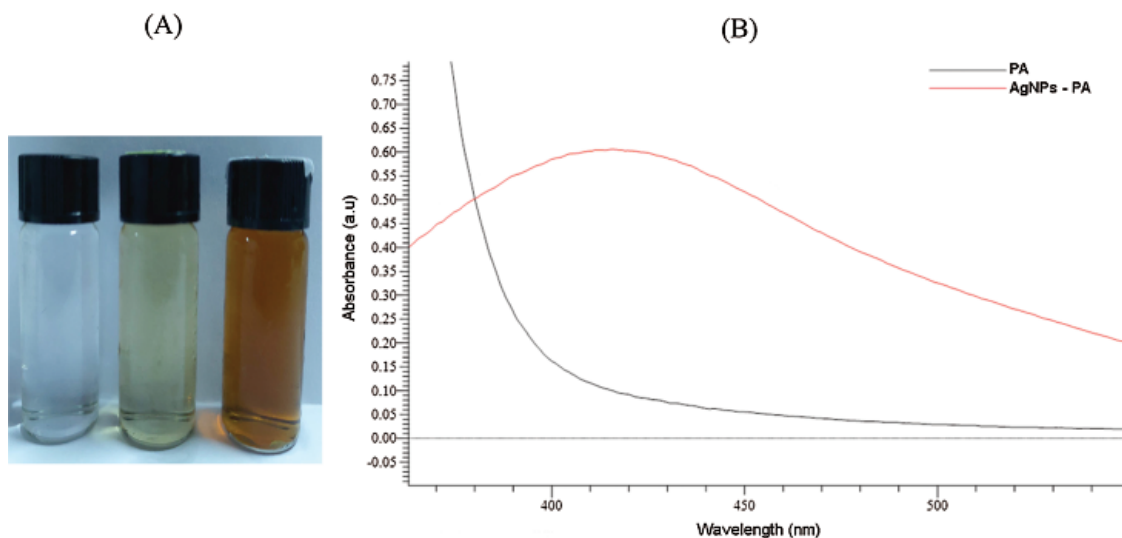


Figure 3: Photograph of AgNO_3 , PA leaf extract and AgNPs-PA (A). UV-vis spectra of PA leaf extract and AgNPs-PA (B)

3.2.2 XRD Analysis

The XRD patterns of AgNPs-PA are shown in Fig. 6A. The XRD analysis of AgNPs-PA showed diffraction peak at $2\theta = 38.13^\circ$, 44.27° , 64.54° , and 77.34° corresponding to (111), (200), (220), and (311) facet of silver crystal, respectively [46,47]. These peaks matched perfectly with the data in JCPDS file. No. 04-0783, confirmed the formation of AgNPs. These values may indicate that AgNPs-PA was indexed to a face-center cubic structure. However, some undefined peaks were also observed at 32.17° (Fig. 6A), 32.19° , 55.81° , 57.44° . These peaks may indicate the presence of some bioorganic traces on the surface of AgNPs. The average crystallite size was calculated from Scherrer's formula [48] Eq. (1):

$$D = \frac{0.9 \times \lambda}{\beta \times \cos \theta} \quad (1)$$

where D is the crystalline domain size, K is the Scherrer constant ($K = 0.9$ in this case), α is the wavelength of the X-ray ($\alpha = 1.574 \times 10^{-10} \text{ m} = 1.54060 \text{ \AA} = 0.154060 \text{ nm}$), β is the peak angular width, and θ is the diffraction angle.

Using XRD data and Debye-Scherrer equation, the average crystal of AgNPs-PA was calculated to be 10.62 nm.

3.2.3 DLS Study

DLS measurements were used to determine the hydrodynamic size of nanoparticles which was presented as an important parameter to understand the size of particles and their performance in biological assays [49]. In previous studies, the particle size of biosynthesized AgNPs using various plants extracts depended on reaction conditions or changing the composition of a reaction mixture [50,51]. The average diameter of AgNPs-PA, calculated from the DLS size distribution images (Fig. 6B) was measured at $65.70 \pm 29.50 \text{ nm}$. It should be noted that the sizes of particles measured using DLS were much higher than those determined from XRD, indicating the adsorption of biochemical of the PA extract onto the surface of particles. This result may be explained by the fact that XRD determined the crystallite sizes in the dried state while DLS was performed on samples in a solvated state to measure the hydrodynamic size.

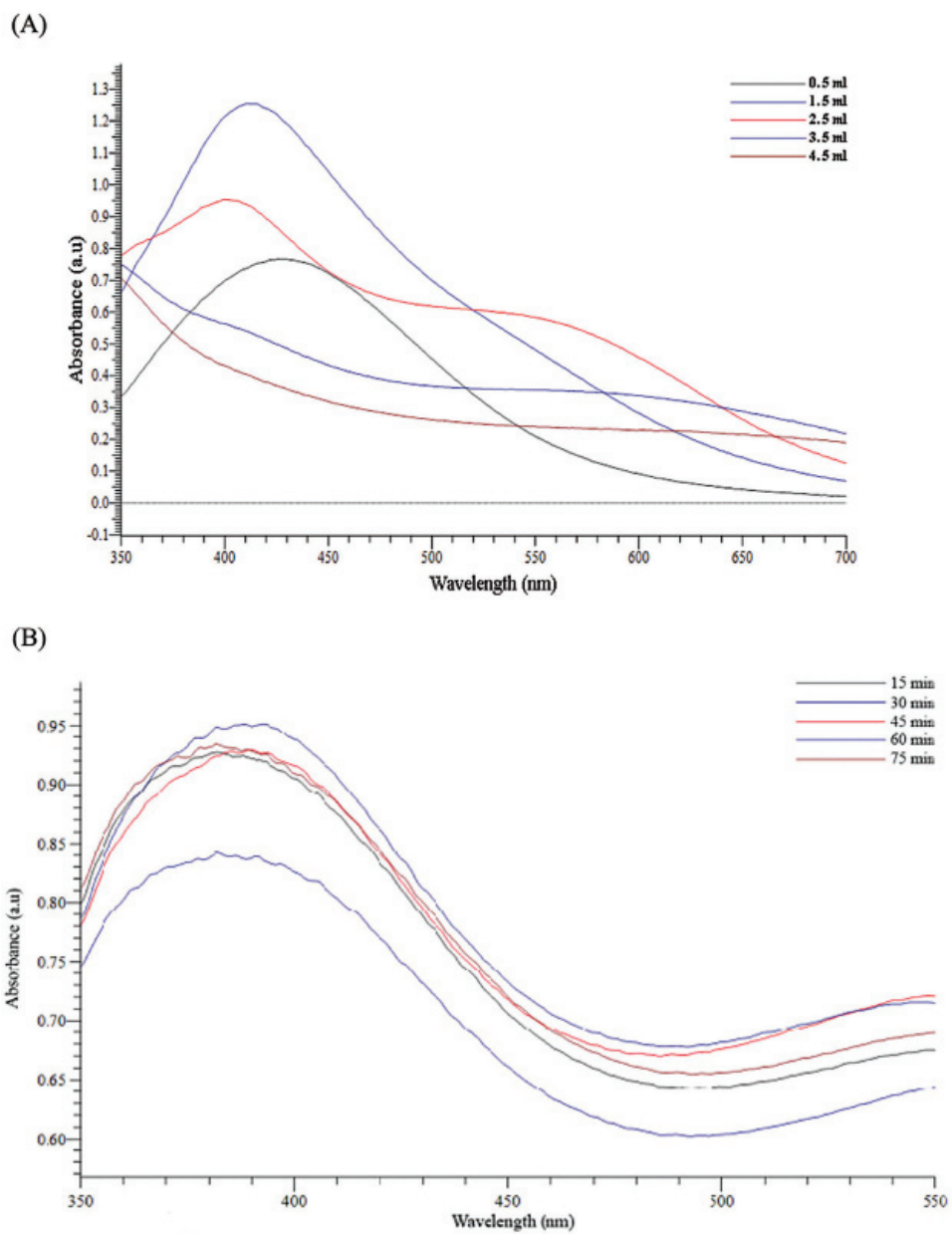


Figure 4: (continued)

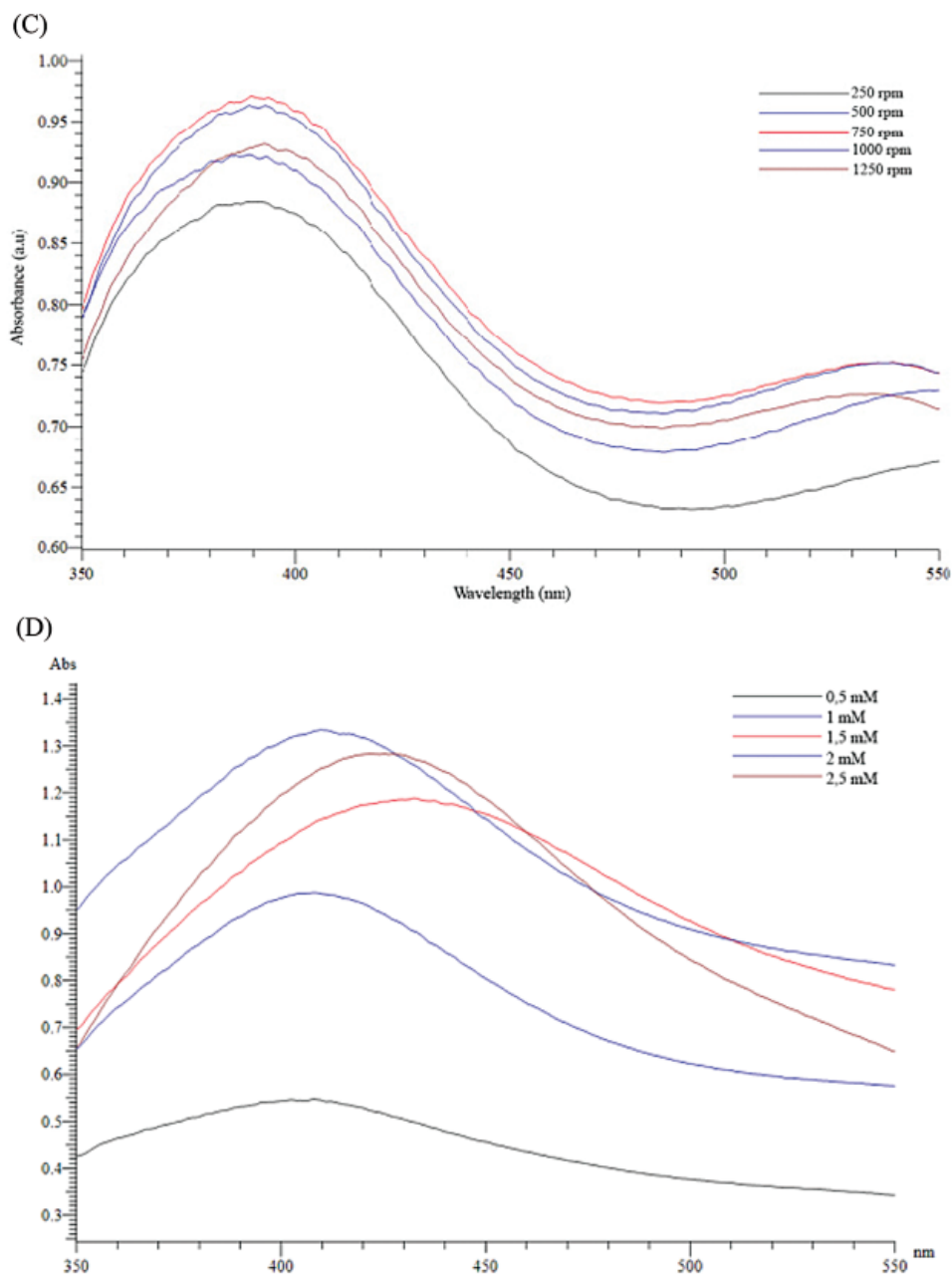


Figure 4: Effects of extract volume of PA (A), the stirring time (B), the stirring rate (C) and silver nitrate concentration (D) on UV-vis spectra of AgNPs-PA

3.2.4 SEM and EDX Study

The surface morphology of PA leaf extract mediated synthesized silver nanoparticles was determined using SEM images (Fig. 7A). AgNPs-PA was uniform and mostly spherical particles without any aggregation and the sizes of particles were about 20.45 nm. This was slightly higher than the values found in XRD. These results were also consistent with those conducted by Reddy et al. [52] and Ajitha et al. [53]. EDX technique was devoted to confirm the presence of element silver (Ag), Carbon (C) and Oxygen (O) in biogenic synthesis of silver nanoparticles (Fig. 7B). These results therefore indicated not

only the successful formation of AgNPs, but also confirmed the phytoconstituents presented in PA leaf extract acted as reducing and capping agents for the synthesis and the stabilization of AgNPs.

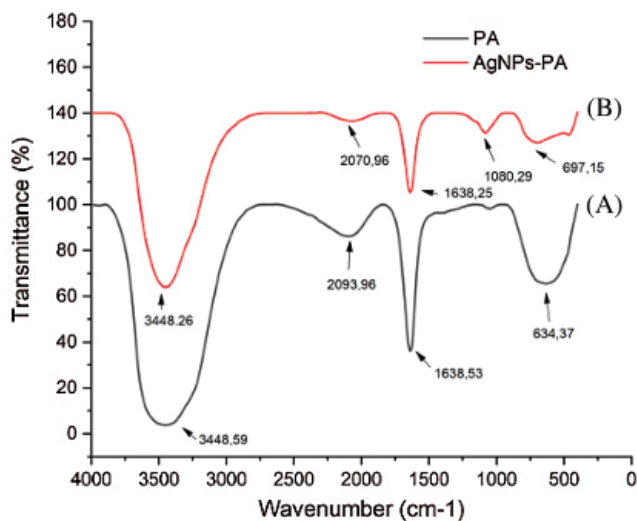


Figure 5: FTIR spectra of (A) PA (black line), (B) AgNPs-PA (red line)

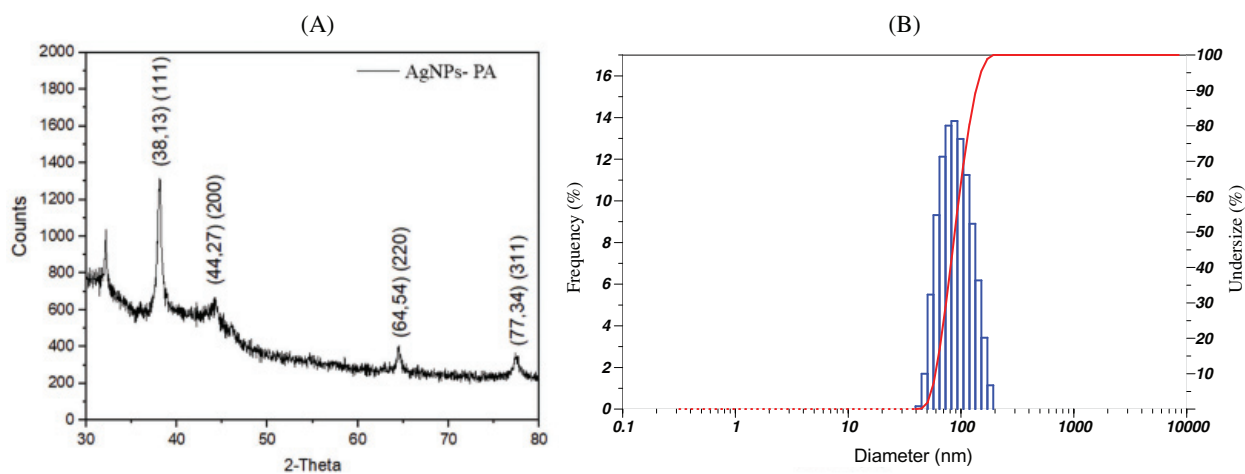


Figure 6: (A) XRD pattern and (B) DLS pattern of AgNPs-PA

3.3 Characterization of CMC/PVA and CMC/PVA-AgNPs Films

XRD spectrum of the CMC/PVA film showed a single large peak at $2\theta = 19.57^\circ$ due to the indexed (101) plane of semicrystalline PVA. Moreover, the peak was broad because it related to the crystalline cellulosic structure of CMC. It was possibly indicated that hydrogen bonding interactions between CMC and PVA were occurred. The presence of AP synthesized AgNPs in CMC/PVA film led to the appearance of diffraction peaks at $2\theta = 32.34^\circ$, 46.45° , 78.01° , which could be indexed to the characteristic peaks (101), (200), and (311) of AgNPs. As the obtained peak values were found be in good agreement with the stated JCPDS file No. 04-0783, the presence of AgNPs in CMC/PVA film could be confirmed.

The surface morphology of the CMC/PVA films with and without AP synthesized AgNPs was investigated using the SEM technique as shown in Figs. 8A and 8B. It was observed that purely

CMC/PVA films exhibited a clear, smooth, and homogeneous surface which indicated a dense structure. The Fig. 8B that related to the CMC/PVA films with silver nanoparticles revealed the surface became slightly rough with appearance of tiny white spots owing to the presence of AgNPs in the films.

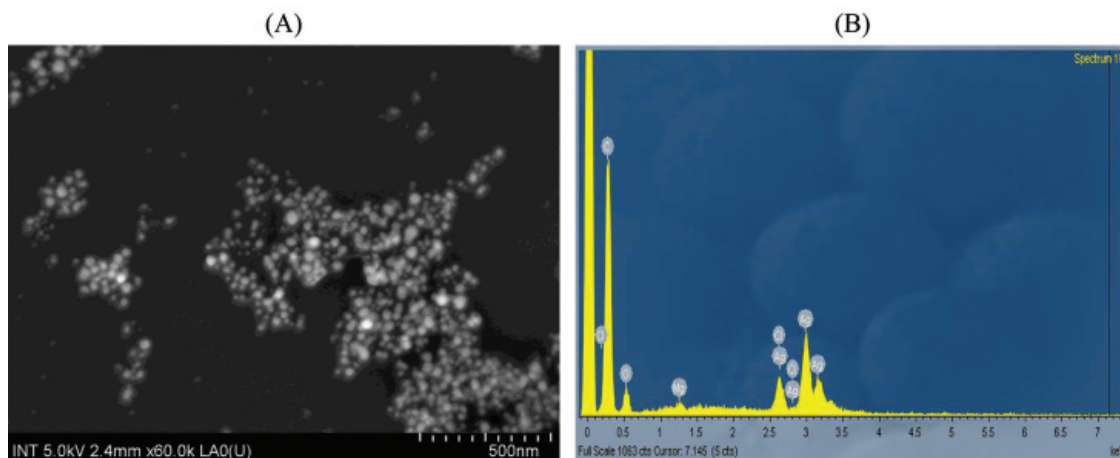


Figure 7: (A) SEM images and (B) EDX pointer of AgNPs-PA

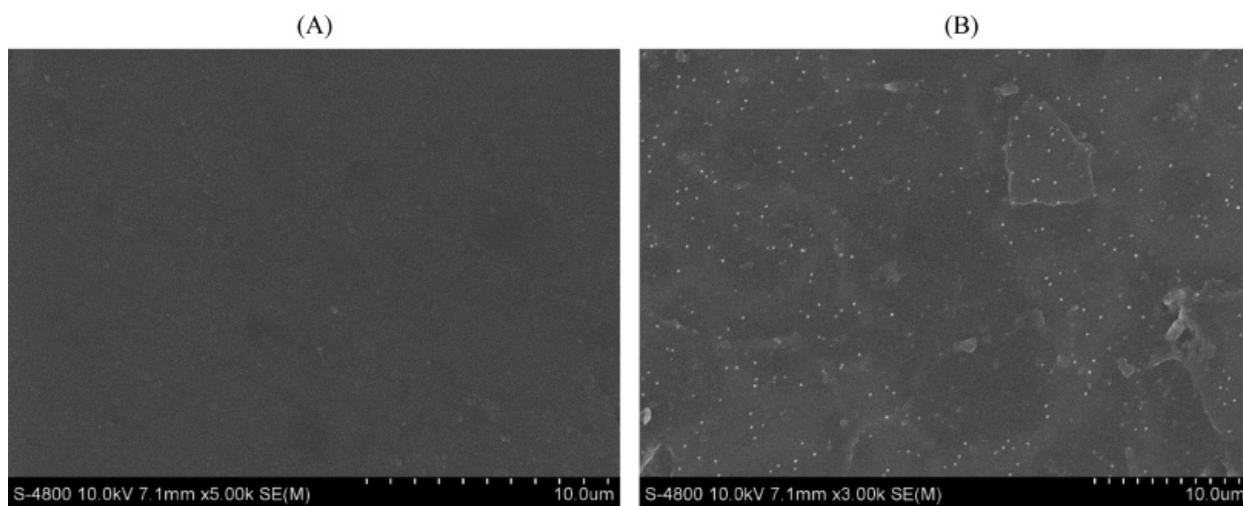


Figure 8: (continued)

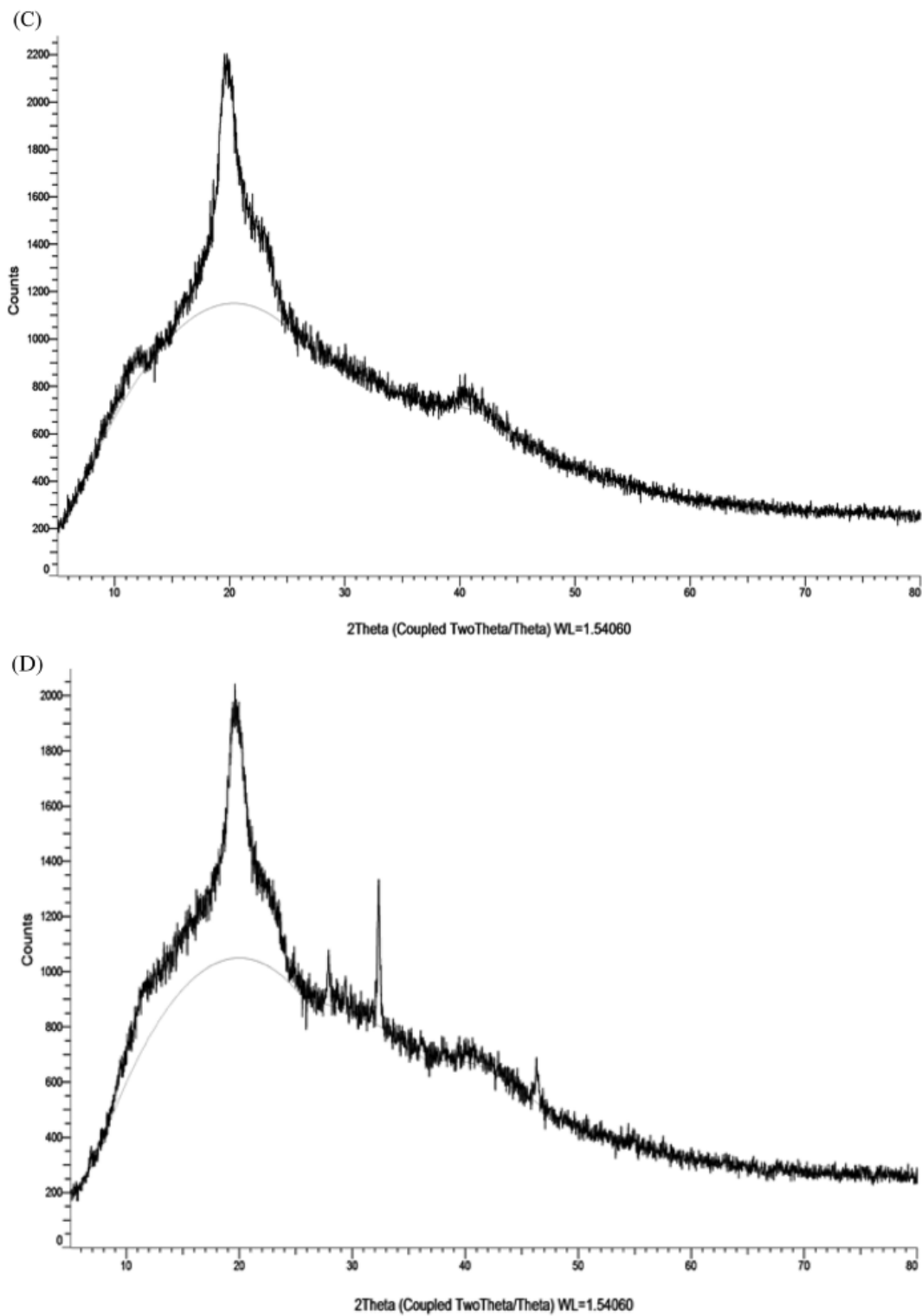


Figure 8: SEM images of PVA/CMC (A) and PVA/CMC-AgNPs films (B). XRD patterns of PVA/CMC (C) and PVA/CMC-AgNPs films (D)

The FT-IR spectra of AgNPs, CMC/PVA films and CMC/PVA-AgNPs nanocomposites were recorded in the range 500 cm^{-1} – 4000 cm^{-1} in order to identify the functional groups of the samples (Fig. 9). Fig. 9 displays the FT-IR spectra of AP synthesized AgNPs. The asymmetric and symmetric stretching vibrations of OH groups for alcohols and phenols occurred around at 3448.26 cm^{-1} . The peak at 1638.25 cm^{-1} assigned to C=O stretching. One peak at 1080.29 cm^{-1} could be attributed CO group of AP leaf extract. The pure CMC/PVA film displayed a strong and broad peak at 3320.88 cm^{-1} which could be ascribed to the stretching vibration of OH groups that involved in the formation of various kinds of intermolecular and intramolecular hydrogen bonds. The band corresponding to the CH asymmetric stretching vibration from alkyl group occurred at 2942.17 cm^{-1} . A peak at 1733.22 cm^{-1} was attributed to CO stretching vibration of vinyl acetate group. Another peak at 1424.85 cm^{-1} and 1376.49 cm^{-1} were associated to the CH bending. The absorbance peak observed at 1095.41 cm^{-1} represented CO stretching of acetyl group. From Fig. 9, it is obvious that the spectra of both the CMC/PVA and CMC/PVA-AgNPs had similar functional groups. However, in the CMC/PVA-AgNPs film, the broadness of OH stretching band at 3453.56 cm^{-1} and the intensity of CH_2 asymmetric stretching band at 2926.52 cm^{-1} was decreased in comparison to that of the pure CMC/PVA. It could be due to the interaction of silver nanoparticles with CMC/PVA.

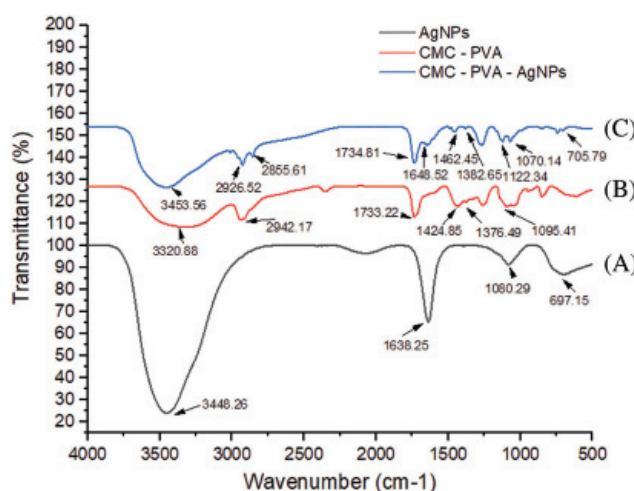


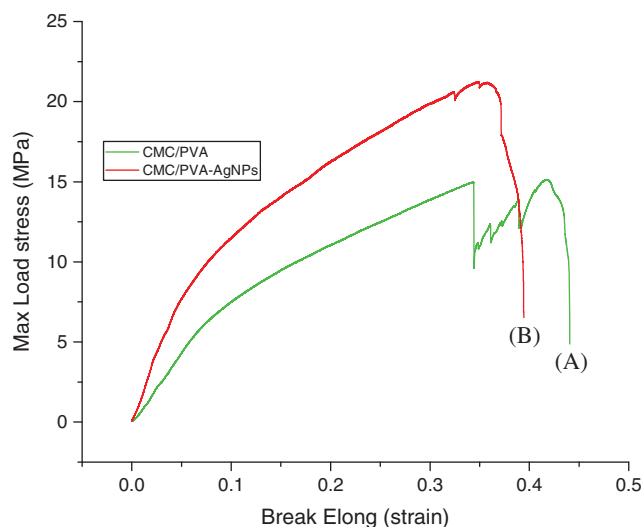
Figure 9: FTIR spectra of (A) AgNPs (black line), (B) CMC/PVA (red line), and (C) CMC/PVA-AgNPs (blue line) films

3.4 Mechanical Properties of CMC/PVA and CMC/PVA-AgNPs Films

The tensile test is one of the most fundamental and essential mechanical tests. Tensile strength and the percentage of elongation at break values are presented in Tab. 1. Fig. 10 shows the average curves of the tensile tests on the CMC/PVA films with and without silver nanoparticles. The results indicated that the average tensile strength of CMC/PVA and CMC/PVA-AgNPs films were determined to be $16.52 \pm 1.38\text{ MPa}$ and $24.07 \pm 2.29\text{ MPa}$, respectively. It is obvious that the incorporation of AgNPs could significantly improve the tensile strength and the percentage of elongation at break with respect to those of CMC/PVA films. It might be due to the fact that silver nanoparticles have a very large specific surface area which can affect interfacial strength and degree of dispersion [54]. In addition, the main reason for this improvement in the mechanical properties of nanocomposites could be the stronger interfacial interaction between the silver nanoparticles and the biopolymer matrix due to the formation of hydrogen and covalent bonds between AgNPs and hydroxyl groups of CMC/PVA films. The existence of these new bonds would improve the mechanical properties of films.

Table 1: Mechanical properties of CMC/PVA and CMC/PVA-AgNPs

Sample	Tensile strength MPa	Elongation %	Elasticity MPa	Thickness mm
CMC/PVA	16.52 ± 1.38	56.27 ± 11.87	77.88 ± 10.87	0.33 ± 0.00
CMC/PVA-AgNPs	24.07 ± 2.29	67.83 ± 8.81	82.28 ± 10.89	0.20 ± 0.00

**Figure 10:** Stress-strain curve of (A) CMC/PVA (green line) and (B) CMC/PVA-AgNPs (red line) films

3.5 Antibacterial Properties of CMC/PVA and CMC/PVA-AgNPs Films

The antimicrobial efficacy of CMC/PVA and CMC/PVA-AgNPs films were determined against panel of bacterial strains using the disk diffusion method. Four common bacterial model strains *i.e.*, gram negative (*Escherichia Coli* and *Salmonella typhi*) and gram positive (*Bacillus spizizenii* and *Staphylococcus aureus*) were used in this research. Fig. 11 showed the results of antimicrobial tests regarding microorganisms and the zone of inhibition of films. The pure CMC/PVA films did not show any bacterial effect against both gram positive and gram negative bacterial. However, CMC/PVA films containing AgNPs had the ability to effectively inhibit and kill the growth of *Bacillus spizizenii*, *Staphylococcus aureus*, *Escherichia Coli* and *Salmonella typhi* bacteria. This was due to the antimicrobial chemical properties of silver nanoparticles in the composite. Tab. 2 showed that the diameters of the zones of inhibition of *Bacillus spizizenii*, *Staphylococcus aureus*, *Escherichia Coli* and *Salmonella typhi* growth were 9.2 ± 0.3 mm, 12.7 ± 0.5 mm, 9.0 ± 0.4 mm and 10.1 ± 0.6 mm, respectively. It was observed that *S. aureus* was quasi-sensitive and resistant to CMC/PVA with silver nanoparticles compared to *E. coli*, as reported by Kim et al. [55]. The possible reason why gram-negative bacteria was less sensitive than gram-positive bacteria to silver nanoparticles might be the difference between the structures of the outer cell membranes of these microorganisms. Also the study conducted by de Moura et al. [56], tested the antibacterial activity of HPMC film containing 41 nm AgNPs against *Escherichia coli* (*E. coli*) and *Staphylococcus aureus* (*S. aureus*), which were 2.75 mm and 3.11 mm, respectively, while results obtained from the present study showed that the zone of inhibitions of CMC/PVA film containing 20.45 nm AgNPs against *E. coli* and *S. aureus* were 10.1 mm and 12.7 mm, respectively. These results clearly demonstrated that in CMC/PVA-AgNPs nanocomposite films possessed good antibacterial

activities against gram positive *S. aureus* as well as gram negative *E.coli*, suggesting their potential for food packaging application.

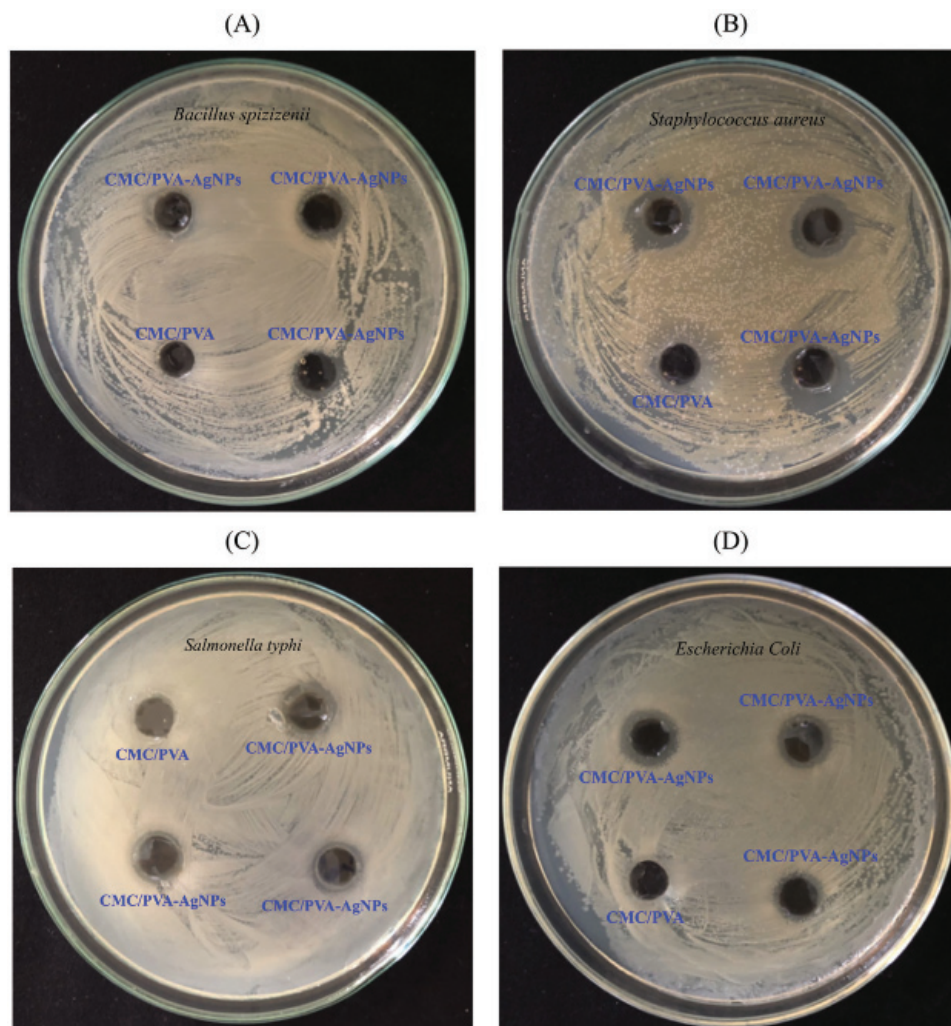


Figure 11: Plates showing the antibacterial activity of fabricated CMC/PVA-AgNPs and CMC/PVA against *Bacillus spizizenii* (plate A), *Staphylococcus aureus* (Plate B), *Salmonella typhi* (Plate C) and *Escherichia Coli* (Plate D)

Table 2: Antibacterial activity of CMC/PVA and CMC/PVA-AgNPs films on microorganisms

Sample	Zone of inhibition (mm)			
	<i>Bacillus spizizenii</i>	<i>Staphylococcus aureus</i>	<i>Salmonella typhi</i>	<i>Escherichia Coli</i>
CMC/PVA	0	0	0	0
CMC/PVA-AgNPs	9.2 ± 0.3	12.7 ± 0.5	9.0 ± 0.4	10.1 ± 0.6

4 Conclusion

The CMC/PVA films with and without silver nanoparticles had been prepared by a solvent casting method. The SEM micrographs showed the modification of the smooth surface morphology of the pure CMC/PVA film to the rough for the nanocomposite CMC/PVA-AgNPs. From the FT-IR results, the interactions between the AgNPs-PA and the OH functional groups of CMC/PVA can be confirmed. The XRD analysis also proved the existence of silver nanoparticles. The mechanical properties of the CMC/PVA film increased with the addition of silver nanoparticles in comparison to those of the pure CMC/PVA films. The obtained data showed that the CMC/PVA films had a tensile strength equal to 16.52 ± 1.38 MPa and this value had been ameliorated to 24.07 ± 2.29 MPa with the addition of AgNPs. The biosynthesis of silver nanoparticles using the extract of *Plectranthus amboinicus* was an eco-friendly and cost-effective approach. The structural nature of the biosynthesized silver nanoparticles had been completely characterized by DLS, UV-vis, FT-IR, SEM, and XRD. FT-IR and UV-vis analyses confirmed the effective synthesis of the silver nanoparticles. The XRD results showed that the silver nanoparticles had the FCC crystal structure with a calculated crystallite size of an order of magnitude of a few tens of nanometers. Finally, the CMC/PVA-AgNPs showed a significant antibacterial activity against *Bacillus spizizenii*, *Staphylococcus aureus*, *Escherichia Coli* and *Salmonella typhi*, and could potentially be used for food packaging application.

Funding Statement: This research was funded by Nong Lam University Ho Chi Minh City, Vietnam under Grant Code CS-CB19-KH-02.

Conflicts of Interest: The authors declare that they have no conflicts of interest to report regarding the present study.

References

1. George, J., Ishida, H. (2018). A review on the very high nanofiller-content nanocomposites: Their preparation methods and properties with high aspect ratio fillers. *Progress in Polymer Science*, 86, 1–39. DOI 10.1016/j.progpolymsci.2018.07.006.
2. Carbone, M., Donia, D. T., Sabbatella, G., Antiochia, R. (2016). Silver nanoparticles in polymeric matrices for fresh food packaging. *Journal of King Saud University-Science*, 28(4), 273–279. DOI 10.1016/j.jksus.2016.05.004.
3. Morsi, M. A., Oraby, A. H., Elshahawy, A. G., Abd El-Hady, R. M. (2019). Preparation, structural analysis, morphological investigation and electrical properties of gold nanoparticles filled polyvinyl alcohol/carboxymethyl cellulose blend. *Journal of Materials Research and Technology*, 8(6), 5996–6010. DOI 10.1016/j.jmrt.2019.09.074.
4. Ernest Ravindran, R. S., Subha, V., Ilangovan, R. (2020). Silver nanoparticles blended PEG/PVA nanocomposites synthesis and characterization for food packaging. *Arabian Journal of Chemistry*, 13(7), 6056–6060. DOI 10.1016/j.arabjc.2020.05.005.
5. Ortega, F., Arce, V. B., Garcia, M. A. (2021). Nanocomposite starch-based films containing silver nanoparticles synthesized with lemon juice as reducing and stabilizing agent. *Carbohydrate Polymers*, 252(2), 117208. DOI 10.1016/j.carbpol.2020.117208.
6. Wang, H., Qiao, X., Chen, J., Ding, S. (2005). Preparation of silver nanoparticles by chemical reduction method. *Colloids and Surfaces, A: Physicochemical and Engineering Aspects*, 256(2-3), 111–115. DOI 10.1016/j.colsurfa.2004.12.058.
7. Khaydarov, R. A., Khaydarov, R. R., Gapurova, O., Estrin, Y., Scheper, T. (2009). Electrochemical method for the synthesis of silver nanoparticles. *Journal of Nanoparticle Research*, 11(5), 1193–1200. DOI 10.1007/s11051-008-9513-x.
8. Navaladian, S., Viswanathan, B., Viswanath, R. P., Varadarajan, T. K. (2007). Thermal decomposition as route for silver nanoparticles. *Nanoscale Research Letters*, 2(1), 44–48. DOI 10.1007/s11671-006-9028-2.

9. Azizian-Shermeh, O., Einali, A., Ghasemi, A. (2017). Rapid biologically one-step synthesis of stable bioactive silver nanoparticles using Osage orange (*Maclura pomifera*) leaf extract and their antimicrobial activities. *Advanced Powder Technology*, 28(12), 3164–3171. DOI 10.1016/j.appt.2017.10.001.
10. Sana, S. S., Dogiparthi, L. K. (2018). Green synthesis of silver nanoparticles using Givotia moluccana leaf extract and evaluation of their antimicrobial activity. *Materials Letters*, 226(3), 47–51. DOI 10.1016/j.matlet.2018.05.009.
11. Hamelian, M., Zangeneh, M. M., Amisama, A., Varmira, K., Veisi, H. (2018). Green synthesis of silver nanoparticles using *Thymus kotschyanus* extract and evaluation of their antioxidant, antibacterial and cytotoxic effects. *Applied Organometallic Chemistry*, 32(9), e4458. DOI 10.1002/aoc.4458.
12. Awwad, A. M., Salem, N. M. (2012). Green synthesis of silver nanoparticles by Mulberry Leaves Extract. *Nanoscience and Nanotechnology*, 2(4), 125–128. DOI 10.5923/j.nn.20120204.06.
13. Nakhjavani, M., Nikkhah, V., Sarafraz, M. M., Shoja, S., Sarafraz, M. (2017). Green synthesis of silver nanoparticles using green tea leaves: Experimental study on the morphological, rheological and antibacterial behaviour. *Heat and Mass Transfer*, 53(10), 3201–3209. DOI 10.1007/s00231-017-2065-9.
14. Mosaviniya, M., Kikhavani, T., Tanzifi, M., Tavakkoli Yaraki, M., Tajbakhsh, P. et al. (2019). Facile green synthesis of silver nanoparticles using *Crocus Haussknechtii* Bois bulb extract: Catalytic activity and antibacterial properties. *Colloid and Interface Science Communications*, 33, 100211. DOI 10.1016/j.colcom.2019.100211.
15. Kambale, E. K., Nkanga, C. I., Mutonkole, B. P. I., Bapolisi, A. M., Tassa, D. O. et al. (2020). Green synthesis of antimicrobial silver nanoparticles using aqueous leaf extracts from three Congolese plant species (*Brillantaisia patula*, *Crossopteryx febrifuga* and *Senna siamea*). *Heliyon*, 6(8), e04493. DOI 10.1016/j.heliyon.2020.e04493.
16. Hemmati, S., Rashtiani, A., Zangeneh, M. M., Mohammadi, P., Zangeneh, A. et al. (2019). Green synthesis and characterization of silver nanoparticles using *Fritillaria* flower extract and their antibacterial activity against some human pathogens. *Polyhedron*, 158, 8–14. DOI 10.1016/j.poly.2018.10.049.
17. Bindhu, M. R., Umadevi, M. (2015). Antibacterial and catalytic activities of green synthesized silver nanoparticles. *Spectrochimica Acta Part A: Molecular and Biomolecular Spectroscopy*, 135(025008), 373–378. DOI 10.1016/j.saa.2014.07.045.
18. Das, P., Ghosal, K., Jana, N. K., Mukherjee, A., Basak, P. (2019). Green synthesis and characterization of silver nanoparticles using belladonna mother tincture and its efficacy as a potential antibacterial and anti-inflammatory agent. *Materials Chemistry and Physics*, 228, 310–317. DOI 10.1016/j.matchemphys.2019.02.064.
19. Hussain, M., Nafady, A., Avci, A., Pehlivan, E., Nisar, J. et al. (2019). Biogenic silver nanoparticles for trace colorimetric sensing of enzyme disrupter fungicide vinclozolin. *Nanomaterials*, 9(11), 1604. DOI 10.3390/nano9111604.
20. Tao, A., Kim, F., Hess, C., Goldberger, J., He, R. et al. (2003). Langmuir–Blodgett Silver Nanowire monolayers for molecular sensing using surface-enhanced Raman Spectroscopy. *Nano Letters*, 3(9), 1229–1233. DOI 10.1021/nl0344209.
21. Kouvaris, P., Delimitis, A., Zaspalis, V., Papadopoulos, D., Tspas, S. A. et al. (2012). Green synthesis and characterization of silver nanoparticles produced using *Arbutus Unedo* leaf extract. *Materials Letters*, 76, 18–20. DOI 10.1016/j.matlet.2012.02.025.
22. Cho, K.-H., Park, J.-E., Osaka, T., Park, S.-G. (2005). The study of antimicrobial activity and preservative effects of nanosilver ingredient. *Electrochimica Acta*, 51(5), 956–960. DOI 10.1016/j.electacta.2005.04.071.
23. Sanpui, P., Murugadoss, A., Prasad, P. V. D., Ghosh, S. S., Chattopadhyay, A. (2008). The antibacterial properties of a novel chitosan-Ag-nanoparticle composite. *International Journal of Food Microbiology*, 124(2), 142–146. DOI 10.1016/j.ijfoodmicro.2008.03.004.
24. Alsammaraie, F. K., Wang, W., Zhou, P., Mustapha, A., Lin, M. (2018). Green synthesis of silver nanoparticles using turmeric extracts and investigation of their antibacterial activities. *Colloids and Surfaces, B: Biointerfaces*, 171, 398–405. DOI 10.1016/j.colsurfb.2018.07.059.
25. Ojo, O. A., Oyinloye, B. E., Ojo, A. B., Afolabi, O. B., Peters, O. A. et al. (2017). Green synthesis of silver nanoparticles (AgNPs) using *Talinum triangulare* (Jacq.) Willd. leaf extract and monitoring their antimicrobial activity. *Journal of Bionanoscience*, 11(4), 292–296. DOI 10.1166/jbns.2017.1452.

26. Chen, X., Yan, J. K., Wu, J. Y. (2016). Characterization and antibacterial activity of silver nanoparticles prepared with a fungal exopolysaccharide in water. *Food Hydrocolloids*, 53(23–24), 69–74. DOI 10.1016/j.foodhyd.2014.12.032.
27. AbdelRahim, K., Mahmoud, S. Y., Ali, A. M., Almaary, K. S., Mustafa, A. E. Z. M. A. et al. (2017). Extracellular biosynthesis of silver nanoparticles using *Rhizopus stolonifer*. *Saudi Journal of Biological Sciences*, 24(1), 208–216. DOI 10.1016/j.sjbs.2016.02.025.
28. Morsi, M. A., Rajeh, A., Menazea, A. A. (2019). Nanosecond laser-irradiation assisted the improvement of structural, optical and thermal properties of polyvinyl pyrrolidone/carboxymethyl cellulose blend filled with gold nanoparticles. *Journal of Materials Science: Materials in Electronics*, 30(3), 2693–2705. DOI 10.1007/s10854-018-0545-4.
29. Choudhary, S. (2018). Characterization of amorphous silica nanofiller effect on the structural, morphological, optical, thermal, dielectric and electrical properties of PVA-PVP blend based polymer nanocomposites for their flexible nanodielectric applications. *Journal of Materials Science: Materials in Electronics*, 29(12), 10517–10534. DOI 10.1007/s10854-018-9116-y.
30. El Sayed, A. M. (2014). Synthesis and controlling the optical and dielectric properties of CMC/PVA blend via γ -rays irradiation. *Nuclear Instruments and Methods in Physics Research, Section B: Beam Interactions with Materials and Atoms*, 321, 41–48. DOI 10.1016/j.nimb.2013.12.020.
31. Cobos, M., De-La-Pinta, I., Quindós, G., Fernández, M. J., Fernández, M. D. (2020). Synthesis, physical, mechanical and antibacterial properties of nanocomposites based on Poly (vinyl alcohol)/Graphene oxide-silver nanoparticles. *Polymers*, 12(3), 723. DOI 10.3390/polym12030723.
32. Kamoun, E. A., Kenawy, E. R. S., Chen, X. (2017). A review on polymeric hydrogel membranes for wound dressing applications: PVA-based hydrogel dressings. *Journal of Advanced Research*, 8(3), 217–233. DOI 10.1016/j.jare.2017.01.005.
33. Jayakumar, A., Heera, K. V., Sumi, T. S., Joseph, M., Mathew, S. et al. (2019). Starch-PVA composite films with zinc-oxide nanoparticles and phytochemicals as intelligent pH sensing wraps for food packaging application. *International Journal of Biological Macromolecules*, 136(1), 395–403. DOI 10.1016/j.ijbiomac.2019.06.018.
34. Rolim, W. R., Pieretti, J. C., Renó, D. L. S., Lima, B. A., Nascimento, M. H. M. et al. (2019). Antimicrobial activity and cytotoxicity to tumor cells of nitric oxide donor and silver nanoparticles containing PVA/PEG films for topical applications. *ACS Applied Materials & Interfaces*, 11(6), 6589–6604. DOI 10.1021/acsami.8b19021.
35. Batool, S., Hussain, Z., Niazi, M. B. K., Liaqat, U., Afzal, M. (2019). Biogenic synthesis of silver nanoparticles and evaluation of physical and antimicrobial properties of Ag/PVA/starch nanocomposites hydrogel membranes for wound dressing application. *Journal of Drug Delivery Science and Technology*, 52(3), 403–414. DOI 10.1016/j.jddst.2019.05.016.
36. Augustine, R., Hasan, A., Yadu Nath, V. K., Thomas, J., Augustine, A. et al. (2018). Electrospun polyvinyl alcohol membranes incorporated with green synthesized silver nanoparticles for wound dressing applications. *Journal of Materials Science: Materials in Medicine*, 29(11), 223. DOI 10.1007/s10856-018-6169-7.
37. Ghaffari-Moghaddam, M., Eslahi, H. (2014). Synthesis, characterization and antibacterial properties of a novel nanocomposite based on polyaniline/polyvinyl alcohol/Ag. *Arabian Journal of Chemistry*, 7(5), 846–855. DOI 10.1016/j.arabjc.2013.11.011.
38. Zulkifli, F. H., Rani, N. A. M., Shahitha, F. (2019). Carboxymethyl cellulose nanofibres impregnated with silver nanoparticles for tissue engineering applications. *Materials Today: Proceedings*, 16, 1715–1721. DOI 10.1016/j.matpr.2019.06.041.
39. Mankad, M., Patil, G., Patel, D., Patel, P., Patel, A. (2020). Comparative studies of sunlight mediated green synthesis of silver nanoparticles from *Azadirachta indica* leaf extract and its antibacterial effect on *Xanthomonas oryzae* pv. *oryzae*. *Arabian Journal of Chemistry*, 13(1), 2865–2872. DOI 10.1016/j.arabjc.2018.07.016.
40. Qais, F. A., Samreen, Ahmad, I. (2018). Broad-spectrum inhibitory effect of green synthesised silver nanoparticles from *Withania somnifera* (L.) on microbial growth, biofilm and respiration: a putative mechanistic approach. *IET Nanobiotechnology*, 12(3), 325–335. DOI 10.1049/iet-nbt.2017.0193.

41. Arumugam, G., Swamy, M. K., Sinniah, U. R. (2016). *Plectranthus amboinicus* (Lour.) Spreng: Botanical, phytochemical, pharmacological and nutritional significance. *Molecules*, 21(4), 369. DOI 10.3390/molecules21040369.
42. Kotakadi, V. S., Rao, Y. S., Gaddam, S. A., Prasad, T. N. V. K. V., Reddy, A. V. et al. (2013). Simple and rapid biosynthesis of stable silver nanoparticles using dried leaves of *Catharanthus roseus*. *Linn. G. Donn and its Anti Microbial Activity. Colloids and Surfaces, B: Biointerfaces*, 105, 194–198.
43. Govindaraju, K., Kiruthiga, V., Kumar, V. G., Singaravelu, G. (2009). Extracellular synthesis of silver nanoparticles by a marine alga, *Sargassum Wightii* Grevilli and their antibacterial effects. *Journal of Nanoscience and Nanotechnology*, 9(9), 5497–5501. DOI 10.1166/jnn.2009.1199.
44. Jena, J., Pradhan, N., Dash, B. P., Sukla, L. B., Panda, P. K. (2013). Biosynthesis and characterization of silver nanoparticles using microalga *Chlorococcum humicola* and its antibacterial activity. *International Journal of Nanomaterials and Biostructures*, 3(1), 1–8.
45. Zheng, Y., Wang, Z., Peng, F., Fu, L. (2017). Biosynthesis of silver nanoparticles by *Plectranthus amboinicus* leaf extract and their catalytic activity towards methylene blue degradation. *Revista Mexicana de Ingeniería Química*, 16(1), 41–45.
46. Anandalakshmi, K., Venugobal, J., Ramasamy, V. (2016). Characterization of silver nanoparticles by green synthesis method using *Petalium murex* leaf extract and their antibacterial activity. *Applied Nanoscience*, 6(3), 399–408. DOI 10.1007/s13204-015-0449-z.
47. Esmaili, F., Koohestani, H., Abdollah-Pour, H. (2020). Characterization and antibacterial activity of silver nanoparticles green synthesized using *Ziziphora clinopodioides* extract. *Environmental Nanotechnology, Monitoring & Management*, 14(1), 100303. DOI 10.1016/j.enmm.2020.100303.
48. Cullity, B. D., Stock, S. R. (2001). *Elements of X-ray diffraction*. Third Edition. Upper Saddle River, NJ: Prentice Hall.
49. Erjaee, H., Rajaian, H., Nazifi, S. (2017). Synthesis and characterization of novel silver nanoparticles using *Chamaemelum nobile* extract for antibacterial application. *Advances in Natural Sciences: Nanoscience and Nanotechnology*, 8(2), 025004. DOI 10.1088/2043-6254/aa690b.
50. Ahmed, S., Saifullah, Ahmad, M., Swami, B. L., Ikram, S. (2019). Green synthesis of silver nanoparticles using *Azadirachta indica* aqueous leaf extract. *Journal of Radiation Research and Applied Sciences*, 9(1), 1–7. DOI 10.1016/j.jrras.2015.06.006.
51. Behravan, M., Hossein Panahi, A., Naghizadeh, A., Ziaee, M., Mahdavi, R. et al. (2019). Facile green synthesis of silver nanoparticles using *Berberis vulgaris* leaf and root aqueous extract and its antibacterial activity. *International Journal of Biological Macromolecules*, 124, 148–154. DOI 10.1016/j.ijbiomac.2018.11.101.
52. Reddy, B. P., Mallikarjuna, K., Narasimha, G., Park, S. H. (2017). *Plectranthus amboinicus*–mediated silver, gold, and silver–gold nanoparticles: Phyto-synthetic, catalytic, and antibacterial studies. *Materials Research Express*, 4(8), 085010. DOI 10.1088/2053-1591/aa80a2.
53. Ajitha, B., Reddy, Y. A. K., Reddy, P. S. (2014). Biosynthesis of silver nanoparticles using *Plectranthus amboinicus* leaf extract and its antimicrobial activity. *Spectrochimica Acta Part A: Molecular and Biomolecular Spectroscopy*, 128, 257–262. DOI 10.1016/j.saa.2014.02.105.
54. Franceschini, I., Selmin, F., Pagani, S., Minghetti, P., Cilurzo, F. (2016). Nanofiller for the mechanical reinforcement of maltodextrins orodispersible films. *Carbohydrate Polymers*, 136(8), 676–681. DOI 10.1016/j.carbpol.2015.09.077.
55. Kim, J. S., Kuk, E., Yu, K. N., Kim, J. H., Park, S. J. et al. (2007). Antimicrobial effects of silver nanoparticles. *Nanomedicine: Nanotechnology, Biology and Medicine*, 3(1), 95–101. DOI 10.1016/j.nano.2006.12.001.
56. de Moura, M. R., Mattoso, L. H. C., Zucolotto, V. (2012). Development of cellulose–based bactericidal nanocomposites containing silver nanoparticles and their use as active food packaging. *Journal of Food Engineering*, 109(3), 520–524. DOI 10.1016/j.jfoodeng.2011.10.030.